



A finite element model for rate-dependent behavior of ferroelectric ceramics

Sang-Joo Kim ^{a,*}, Qing Jiang ^b

^a Department of Mechanical and Information Engineering, University of Seoul, 90 Cheonnon-g-dong, Tongdaemun-gu, Seoul 130-743, South Korea

^b Department of Mechanical Engineering, University of California, Riverside, CA 92521, USA

Received 1 October 2000; in revised form 1 May 2001

Abstract

In this article, materials within a crystallite are modeled by continuum particles consisting of various types of ferroelectric variants which are characterized by their mass fractions. The constitutive behavior of each type of variant is characterized by a proposed Helmholtz free energy potential. Polarization switching is modeled by continuous changes of mass fractions which are governed by an onset criterion and a kinetic relation. A finite element algorithm is developed using the virtual work principle. The simulated results on the rate dependence in the polarization and strain responses to applied alternating electric field of different frequencies are in qualitative consistence with experimental observations. The rate-dependent behavior is explained in terms of changes of mass fractions of the variants that polarization switching involves, in response to the loading programs of different loading rates. © 2002 Elsevier Science Ltd. All rights reserved.

Keywords: Rate-dependent switching; Ferroelectric ceramics; Finite element method

1. Introduction

Ferroelectric materials (Jaffe et al., 1971) such as barium titanate, PZT, and PLZT ceramics have been widely used to design various types of smart systems, memory devices, MEMS, etc. The switching property of the materials plays an important role in the operation of some of those systems. In a tetragonal unit cell, the polarization switching occurs when an applied electric field exceeds the coercive field (which is the magnitude of electric field at zero polarization intensity on the electric field–electric displacement hysteresis response) and thus moves the central ion from one of the six off-center tetragonal sites to another. This changes the polar direction to the one that is most closely aligned with the applied electric field. In a polycrystalline ceramic, a crystallite usually has six different types of variants that are combined to form a complicated domain structure/pattern. Therefore, switching process is much more complicated in a polycrystalline material than in a unit cell.

* Corresponding author. Tel.: +11-822-2210-2757; fax: +11-822-2248-5110.

E-mail address: sjk@uos.ac.kr (S.-J. Kim).

It is of interest to model the behavior of these polycrystalline materials at the level of crystallites. This mesoscale model is needed to improve understanding the macroscopic effect of ferroelectric domain switching and to predict the macroscopic behavior of polycrystals by averaging the behavior of each crystallite. Together with experimental observations and measurements, these can provide guidance in the development of constitutive relations.

The finite element method has been used as a powerful tool for analyzing a complicated system. Recently some significant progress has been made in the finite element modeling of ferroelectric materials. A macroscale finite element model for an electro-mechanically coupled material has been suggested by Ghandi and Hagwood (1996, 1997). They formulated a three-dimensional (3-D) eight-node element with nodal displacement and electric potential degrees of freedom using isoparametric shape functions. The phase/polarization state of materials is represented by internal variables in each element, which are updated at each simulation step based on a phenomenological model. A mesoscale finite element model has been developed by Hwang and McMeeking (1998, 1999) and Huo and Jiang (1997, 1998). The former modeled each crystallite as an element with only one type of variant, with the tetragonal orientation for each element selected randomly. When an element satisfies a given switching criterion, switching occurs in the element and the tetragonal axis changes to a different permitted direction immediately. The latter modeled a crystallite as a body of mixture consisting of distinct types of variants and characterized a grain by the values of mass fractions of variants. The mass fractions are regarded as internal variables and updated at each simulation step by a switching criterion.

It has been evident experimentally that the macroscopic behavior of polycrystalline ferroelectric materials is generally rate dependent. For instance, the coercive field becomes increasingly larger with the increasingly higher frequency of the applied alternating electric field, within the frequency range: 1–100 Hz, as reported by Jiang et al. (1994). The above-mentioned models were not developed to model the rate-dependent behavior, although they have been successful in explaining some aspects of ferroelectric domain switching. The present work is to develop a finite element model for the rate-dependent behavior of ferroelectric ceramics associated with domain switching. We model a ferroelectric polycrystalline body as an aggregate of many crystallites with randomly distributed crystal orientations and we partition each crystallite into finite elements. As in Huo and Jiang (1997, 1998), we regard a finite element as a continuum body of mixture characterized by the mass fractions of the existing variants. To model the rate-dependent behavior, we replace the Huo–Jiang switching criterion, that forces finite jumps in mass fractions when switching takes place, by a kinetic relation that leads to continuous evolutions of the mass fractions. This allows us to model the rate dependence of polarization and strain in response to applied alternating electric fields and applied alternating mechanical loads as well.

2. Helmholtz free energy

In the present model, a polycrystalline ferroelectric ceramic is composed of many crystallites with distinct crystal orientation. Furthermore, each crystallite consists of various kinds of variants and has a complicated domain structure. A domain is a region within which there exists only one kind of variant and the polar direction is different from those of neighboring domains. Therefore, in order to understand the behavior of a ferroelectric ceramic, it is necessary to describe the characteristics of each variant in a crystallite of the ceramic. In this section we describe the electro-mechanical behavior of a variant within a crystallite. Many ferroelectric ceramics, such as BaTiO₃ and some PZT solutions, have a tetragonal crystal structure at room temperature, so that a crystallite in these materials may have at most six different types of variants. We assume that each variant can be modeled as a polarizable solid, characterized by the Helmholtz free energy function $\psi_i(\mathbf{p}_i, \mathbf{S}_i)$. The Helmholtz free energy function $\psi_i(\mathbf{p}_i, \mathbf{S}_i)$ for the i -type variant is given by

$$\rho\psi_i(\mathbf{p}_i, \mathbf{S}_i) = \frac{1}{2}\chi_i^S(\mathbf{p}_i - \mathbf{p}_i^s) \cdot (\mathbf{p}_i - \mathbf{p}_i^s) + \frac{1}{2}\mathbf{c}_i^P(\mathbf{S}_i - \mathbf{S}_i^s) \cdot (\mathbf{S}_i - \mathbf{S}_i^s) + \mathbf{H}_i^T(\mathbf{p}_i - \mathbf{p}_i^s) \cdot (\mathbf{S}_i - \mathbf{S}_i^s), \quad (1)$$

where χ_i^S is the inverse dielectric susceptibility tensor of second order at constant strain; \mathbf{c}_i^P the elastic stiffness tensor of fourth order at constant polarization; \mathbf{H}_i the piezoelectric tensor of third order; and \mathbf{p}_i^s and \mathbf{S}_i^s are the spontaneous polarization vector and spontaneous strain tensor of the i -type variant, respectively. The superscript T stands for the transpose of a tensor.

Then the electric field intensity \mathbf{E}_i and stress field \mathbf{T}_i , constitutively related to the Helmholtz free energy function ψ_i by $\mathbf{E}_i = \rho(\partial\psi_i/\partial\mathbf{p}_i)$ and $\mathbf{T}_i = \rho(\partial\psi_i/\partial\mathbf{S}_i)$, are, respectively, given by

$$\begin{aligned} \mathbf{E}_i &= \chi_i^S(\mathbf{p}_i - \mathbf{p}_i^s) + \mathbf{H}_i(\mathbf{S}_i - \mathbf{S}_i^s), \\ \mathbf{T}_i &= \mathbf{c}_i^P(\mathbf{S}_i - \mathbf{S}_i^s) + \mathbf{H}_i^T(\mathbf{p}_i - \mathbf{p}_i^s). \end{aligned} \quad (2)$$

The inversion of these relations leads to

$$\begin{aligned} \mathbf{p}_i &= \mathbf{p}_i^s + \mathbf{y}_i^T \mathbf{E}_i + \mathbf{d}_i \mathbf{T}_i, \\ \mathbf{S}_i &= \mathbf{S}_i^s + \mathbf{s}_i^E \mathbf{T}_i + \mathbf{d}_i^T \mathbf{E}_i, \end{aligned} \quad (3)$$

where \mathbf{y}_i^T , \mathbf{d}_i , and \mathbf{s}_i^E are the dielectric susceptibility tensor at constant stress, piezoelectric tensor and elastic compliance tensor at constant electric field of the i -type variant, respectively. The electric displacement vector \mathbf{D}_i is given by

$$\mathbf{D}_i = \epsilon_i^T \mathbf{E}_i + \mathbf{d}_i \mathbf{T}_i + \mathbf{p}_i^s, \quad (4)$$

where ϵ_i^T is the permittivity tensor of the i -type variant at constant stress given by

$$\epsilon_i^T = \epsilon_0 \mathbf{1} + \mathbf{y}_i^T, \quad (5)$$

where ϵ_0 is the permittivity of free space and $\mathbf{1}$ is the unit tensor. For finite element formulation it is necessary to write \mathbf{D}_i and \mathbf{T}_i in terms of \mathbf{E}_i and \mathbf{S}_i . Then, from Eqs. (3) and (4),

$$\begin{aligned} \mathbf{D}_i &= \epsilon_i^S \mathbf{E}_i + \mathbf{e}_i(\mathbf{S}_i - \mathbf{S}_i^s) + \mathbf{p}_i^s, \\ \mathbf{T}_i &= \mathbf{c}_i^E(\mathbf{S}_i - \mathbf{S}_i^s) - \mathbf{e}_i^T \mathbf{E}_i, \end{aligned} \quad (6)$$

where ϵ_i^S is the permittivity tensor at constant strain, \mathbf{e}_i is the piezoelectric tensor, and \mathbf{c}_i^E the elastic stiffness tensor at constant electric field.

A domain switching can be viewed as a jumping process of dipoles from a high energy state to a low energy state. Therefore, it is necessary to define a potential energy function per unit reference volume $G_i(\mathbf{p}_i, \mathbf{S}_i; \mathbf{E}, \mathbf{T})$ of the i -type variant by

$$G_i(\mathbf{p}_i, \mathbf{S}_i; \mathbf{E}, \mathbf{T}) = \rho\psi_i(\mathbf{p}_i, \mathbf{S}_i) - \mathbf{E} \cdot \mathbf{p}_i - \mathbf{T} \cdot \mathbf{S}_i. \quad (7)$$

Its value at an extremum of $G_i(\cdot, \cdot; \mathbf{E}, \mathbf{T})$ coincides with the Gibbs free energy per unit reference volume $g_i(\mathbf{p}_i, \mathbf{S}_i)$ of the variant

$$g_i(\mathbf{p}_i, \mathbf{S}_i) = \rho\psi_i(\mathbf{p}_i, \mathbf{S}_i) - \mathbf{E}_i \cdot \mathbf{p}_i - \mathbf{T}_i \cdot \mathbf{S}_i, \quad (8)$$

where \mathbf{E}_i and \mathbf{T}_i are given by Eq. (2). Combining Eq. (8) with Eqs. (1) and (2) yields in terms of \mathbf{p}_i and \mathbf{S}_i

$$g_i(\mathbf{p}_i, \mathbf{S}_i) = -\frac{1}{2}\mathbf{E}_i \cdot (\mathbf{p}_i + \mathbf{p}_i^s) - \frac{1}{2}\mathbf{T}_i \cdot (\mathbf{S}_i + \mathbf{S}_i^s). \quad (9)$$

Inserting Eq. (3) into Eq. (8) gives the Gibbs energy function g_i in terms of \mathbf{E}_i and \mathbf{T}_i as

$$g_i(\mathbf{E}_i, \mathbf{T}_i) = -\frac{1}{2}\mathbf{y}_i^T \mathbf{E}_i \cdot \mathbf{E}_i - \frac{1}{2}\mathbf{s}_i^E \mathbf{T}_i \cdot \mathbf{T}_i - \mathbf{d}_i^T \mathbf{E}_i \cdot \mathbf{T}_i - \mathbf{E}_i \cdot \mathbf{p}_i^s - \mathbf{T}_i \cdot \mathbf{S}_i^s. \quad (10)$$

3. Averaging

The domain structure in a crystallite is so complicated that it is impractical for a continuum-based model for characterizing the behavior of individual domains in the crystallite. Therefore, in order to describe a domain switching, a crystallite is modeled as a continuum body in which a macroscopic particle is smaller than a crystallite but bigger than a domain. A macroscopic particle consists of six distinct types of variants in general and the mass fraction of each type of variant in the particle changes as external loads change. Therefore the process of domain switching can be described by the change in mass fractions of various types of variants in a particle. The mass fraction m_i of the i -type variant in a particle must satisfy the following constraints:

$$0 \leq m_i \leq 1, \quad \sum_{i=1}^6 m_i = 1. \quad (11)$$

Since a crystallite with various types of variants is modeled as a continuum, it is necessary to determine its average physical properties. Recently a number of studies have been done on obtaining the average properties of electro-mechanical materials. Most of them, unfortunately, involve extensive amount of computational work and therefore they are not suitable for the present study dealing with hundreds of crystallites. Here we adopt the simple averaging method, suggested by Huo and Jiang (1998), and assume that all the variants in the same particle are subjected to the same electric and stress fields and that the polarization and strain of the particle are the summation of those of all the variants of the particle weighted by their mass fractions. That is,

$$\mathbf{E}_i = \mathbf{E}, \quad \mathbf{T}_i = \mathbf{T}, \quad (12)$$

$$\psi = \sum_{i=1}^6 m_i \psi_i. \quad (13)$$

$$\mathbf{p} = \sum_{i=1}^6 m_i \mathbf{p}_i, \quad \mathbf{S} = \sum_{i=1}^6 m_i \mathbf{S}_i. \quad (14)$$

Combining Eqs. (1)–(3), (11)–(14) yields

$$\rho \psi(\mathbf{p}, \mathbf{S}) = \frac{1}{2} \boldsymbol{\chi}^S (\mathbf{p} - \mathbf{p}^s) \cdot (\mathbf{p} - \mathbf{p}^s) + \frac{1}{2} \mathbf{c}^P (\mathbf{S} - \mathbf{S}^s) \cdot (\mathbf{S} - \mathbf{S}^s) + \mathbf{H}^T (\mathbf{p} - \mathbf{p}^s) \cdot (\mathbf{S} - \mathbf{S}^s), \quad (15)$$

and

$$\mathbf{p} = \mathbf{p}^s + \mathbf{y}^T \mathbf{E} + \mathbf{d} \mathbf{T}, \quad \mathbf{S} = \mathbf{S}^s + \mathbf{s}^E \mathbf{T} + \mathbf{d}^T \mathbf{E}, \quad (16)$$

where the dielectric susceptibility tensor at constant stress \mathbf{y}^T , the piezoelectric tensor \mathbf{d} , and the elastic compliance tensor at constant electric field \mathbf{s}^E are defined by

$$\begin{aligned} \mathbf{y}^T &= \sum_{i=1}^6 m_i \mathbf{y}_i^T, \\ \mathbf{d} &= \sum_{i=1}^6 m_i \mathbf{d}_i, \\ \mathbf{s}^E &= \sum_{i=1}^6 m_i \mathbf{s}_i^E. \end{aligned} \quad (17)$$

Now we describe the governing equations for the behavior of ferroelectric ceramics using the average quantities defined through Eqs. (14) and (17). According to Coulomb's law and mechanical equilibrium, the average total electric displacement vector \mathbf{D} and the stress tensor \mathbf{T} should be divergence free within a crystallite or a finite element.

$$\operatorname{div} \mathbf{D} = 0, \quad \operatorname{div} \mathbf{T} = 0. \quad (18)$$

The average electric displacement vector \mathbf{D} is given by

$$\mathbf{D} = \epsilon^T \mathbf{E} + \mathbf{d} \mathbf{T} + \mathbf{p}^s, \quad (19)$$

where ϵ^T is the average permittivity tensor at constant stress given by

$$\epsilon^T = \epsilon_0 \mathbf{1} + \mathbf{y}^T, \quad (20)$$

where ϵ_0 is the permittivity of free space and $\mathbf{1}$ is the unit tensor. Eqs. (2) and (6) can be rewritten in terms of average variables and average properties as

$$\begin{aligned} \mathbf{E} &= \chi^S (\mathbf{p} - \mathbf{p}^s) + \mathbf{H} (\mathbf{S} - \mathbf{S}^s), \\ \mathbf{T} &= \mathbf{c}^P (\mathbf{S} - \mathbf{S}^s) + \mathbf{H}^T (\mathbf{p} - \mathbf{p}^s), \end{aligned} \quad (21)$$

or equivalently

$$\begin{aligned} \mathbf{D} &= \epsilon^S \mathbf{E} + \mathbf{e} (\mathbf{S} - \mathbf{S}^s) + \mathbf{p}^s, \\ \mathbf{T} &= \mathbf{c}^E (\mathbf{S} - \mathbf{S}^s) - \mathbf{e}^T \mathbf{E}. \end{aligned} \quad (22)$$

The various average properties shown in Eqs. (21) and (22) are related to each other and the relations can be obtained from a thermodynamical consideration.

Continuity of electric displacement and stress at crystallite or finite element boundaries requires that

$$(\overset{+}{\mathbf{D}} - \overset{-}{\mathbf{D}}) \cdot \mathbf{n} = 0, \quad (\overset{+}{\mathbf{T}} - \overset{-}{\mathbf{T}}) \mathbf{n} = 0, \quad (23)$$

where \mathbf{n} denotes the unit vector normal to the boundary. $(\overset{+}{\cdot})$ and $(\overset{-}{\cdot})$ stand for the limiting values of a generic field quantity (\cdot) at a point on the boundary as the boundary is approached from either side. The average electric field vector \mathbf{E} is given by

$$\mathbf{E} = -\operatorname{grad} \phi, \quad (24)$$

where ϕ is the electric potential. Continuity of electric potential across the boundaries between crystallites or finite elements requires that

$$\overset{+}{\phi} - \overset{-}{\phi} = 0. \quad (25)$$

4. Switching criterion and kinetics

In this section we describe the switching criterion and kinetic relation that are to be utilized in the calculations. The switching criterion determines the conditions under which a domain switching commences. Once a domain switching occurs, its rate is controlled by a kinetic relation. We generalize a viewpoint on the switching criterion and kinetics, suggested by Abeyaratne et al. (1994), and adopted by many researchers including Jiang (1994), and Kim (1998, 2000), that postulates that a phase transformation begins with the nucleation of a new phase out of an old phase and it proceeds at the expense of the old phase. The new phase grows as the phase boundary between the new and old phases migrates in the material body. In their 1-D model, a new phase is nucleated at a critical value of driving force acting on the

phase boundary, and the propagation speed of the phase boundary is determined by the magnitude and direction of driving force. The driving force is the difference in Gibbs energies of the two phases involved in the phase transformation. In a 1-D model, the location of phase boundary acts as an internal variable indicating the progress of phase transformation. However, here in a 3-D model, the mass fractions of variants are used as internal variables, and hence a kinetic relation tells us the rate of change of mass fraction at a given driving force. Next we introduce driving force and describe the switching criterion and kinetics.

4.1. Driving force

In order to describe switching criterion and kinetics it is necessary to define the driving force between two different types of variants. The driving force f_{ij} between the i - and j -type variants is defined by

$$f_{ij} = g_i - g_j, \quad (26)$$

where g_i stands for the Gibbs energy of the i -type variant given by Eq. (8). Therefore, the driving force f_{ij} represents the excess of the Gibbs free energy associated with the i -type variant over that associated with the j -type variant. Abeyaratne et al. (1994), Jiang (1993), and Kim (2000) have shown that in a 1-D setting the second law of thermodynamics requires that the product of driving force acting on a phase boundary and the velocity of phase boundary be greater than or equal to zero. This means a phase transformation should proceed in the way that the total Gibbs energy is decreased. In the present model the requirement of the second law would be generalized to

$$f_{ij} \dot{m}_{ij} \geq 0, \quad (27)$$

where \dot{m}_{ij} stands for the rate of change in the mass fraction of the j -type variant in the $i \rightarrow j$ domain switching. Eq. (27) says that if the Gibbs energy of the i -type variant is higher than that of the j -type variant, then f_{ij} is bigger than zero and from Eq. (27) the i -type variant, if switched, has to be switched to the j -type variant.

4.2. Switching criterion

Many experiments show that a domain switching begins at a critical value of applied field and that this critical value is relatively more certain for a single crystal than for a polycrystalline ceramic (see Hwang et al., 1995; Jona and Shirane, 1962; Strukov and Levanyuk, 1998). Based on those experimental observations, we assume that there exists a critical value of driving force f_{nucl} for the onset of domain switching. That is, the switching criterion for the $i \rightarrow j$ domain switching is given by

$$f_{ij} \geq f_{\text{nucl}} \quad \text{for the onset of } i \rightarrow j \text{ domain switching.} \quad (28)$$

In addition, we assume that if more than one variant satisfies Eq. (28), then the variant with the lowest Gibbs energy is nucleated. For illustration, consider a domain switching in an element consisting of an i -type variant only initially. The application of an external field changes the stability of various variants, including the i -type variant. Suppose that under the applied field a particular variant, for instance the j -type variant, has the smallest Gibbs energy among all the variants. Then, according to the proposed switching criterion, the j -type variant is nucleated from the i -type variant at the instant when the driving force f_{ij} between the two variants reaches the critical value f_{nucl} .

4.3. Kinetics

Once the j -type variant is nucleated out of the parent i -type variant, it grows at the expense of the parent variant at a rate given by a kinetic relation. In this paper we propose a simple linear kinetic relation of frictional type given as follows:

$$\dot{m}_{ij} = \begin{cases} R_{ij}(f_{ij} + f_{cr}) & \text{for } f_{ij} \leq -f_{cr}, \\ 0 & \text{for } -f_{cr} \leq f_{ij} \leq f_{cr}, \\ R_{ij}(f_{ij} - f_{cr}) & \text{for } f_{ij} \geq f_{cr}, \end{cases} \quad (29)$$

where $R_{ij} > 0$ is a material constant representing the flexibility of the $i \rightarrow j$ domain switching and f_{cr} is the critical value of driving force at which the domain switching begins by the movement of domain boundary. For simplicity we assume that R_{ij} is the same for domain switching involving all types of variants of the same material. Since \dot{m}_{ij} represents the rate of $i \rightarrow j$ domain switching, the rate of the reverse $j \rightarrow i$ domain switching \dot{m}_{ji} is $\dot{m}_{ji} = -\dot{m}_{ij}$. The total growth rate of j -type domain \dot{m}_j is given by

$$\dot{m}_j = \sum_{i=1, i \neq j}^6 \dot{m}_{ij}, \quad j = 1, \dots, 6. \quad (30)$$

In finite element calculations, it often happens that the total Gibbs energy of a body is increased after the kinetic relation (29) is applied to all the finite elements satisfying the switching criterion (28). This is contrary to the second law and has to be avoided. One may avoid this contradiction by searching for the different configuration of the body that gives the lowest total Gibbs energy. The details will be discussed in next section.

5. Numerical algorithm

In this section we propose and explain the numerical algorithm that we use in our calculations. The main tool for numerical calculations is the finite element method. The equations for our finite element formulation are developed from the following principle of virtual work:

$$\int_V \delta \mathbf{S} \cdot \mathbf{T} dV + \int_V \delta \mathbf{E} \cdot \mathbf{D} dV = \int_S \delta \mathbf{u} \cdot \mathbf{t} dS + \int_S \delta \phi q dS, \quad (31)$$

where $\delta(\cdot)$ indicates a virtual variation. The mechanical boundary conditions are

$$\begin{aligned} \mathbf{Tn} &= \mathbf{t}_0 & \text{on } S_t, \\ \mathbf{u} &= \mathbf{u}_0 & \text{on } S_u, \end{aligned} \quad (32)$$

where \mathbf{t}_0 is the traction vector given on S_t and \mathbf{u}_0 is the displacement vector given on S_u with $S_u + S_t = S$. The electrical boundary conditions are

$$\begin{aligned} \mathbf{D} \cdot \mathbf{n} &= -q_0 & \text{on } S_q, \\ \phi &= \phi_0 & \text{on } S_\phi, \end{aligned} \quad (33)$$

where ϕ_0 is the prescribed electric potential on S_ϕ and q_0 is the prescribed charge on S_q with $S_\phi + S_q = S$. The displacement and potential fields can be written in terms of finite element interpolations using a matrix notation as

$$\begin{aligned} \{u\} &= [N_u] \{u_N\}, \\ \phi &= \{N_\phi\}^T \{\phi_N\}, \end{aligned} \quad (34)$$

where the matrices $[N_u]$ and $\{N_\phi\}^T$ contain interpolation functions and the matrices $\{u_N\}$ and $\{\phi_N\}$ contain the displacements and potentials respectively for all the nodal points in the finite element mesh. The notation $\{\cdot\}$ stands for a column matrix and the superscript T stands for the transpose of a matrix. The strain matrix $\{S\}$ and electric field vector $\{E\}$ for each element are given by

$$\begin{aligned}\{S\} &= [B_u]\{u_N\}, \\ \{E\} &= -[B_\phi]\{\phi_N\},\end{aligned}\quad (35)$$

where the matrices $[B_u]$ and $[B_\phi]$ result from differentiation of the matrices $[N_u]$ and $\{N_\phi\}$ respectively. Rewriting the constitutive equation (22) using a matrix notation, we get

$$\begin{aligned}\{D\} &= [\epsilon^S]\{E\} + [e](\{S\} - \{S^s\}) + \{p^s\}, \\ \{T\} &= [c^E](\{S\} - \{S^s\}) - [e]^T\{E\}.\end{aligned}\quad (36)$$

Then the matrix equations (34)–(36) are inserted into the virtual work principle (31). Finally using the requirement that the resulting equation must be true for all virtual variations of nodal displacements $\{\delta u_N\}$ and nodal potentials $\{\delta \phi_N\}$, then it follows that the finite element equations are

$$\begin{aligned}[K_{uu}]\{u_N\} + [K_{u\phi}]\{\phi_N\} &= \{F\} + \{F_s\}, \\ [K_{\phi u}]\{u_N\} + [K_{\phi\phi}]\{\phi_N\} &= \{Q\} + \{Q_s\} + \{C\},\end{aligned}\quad (37)$$

where $[K_{uu}]$ and $[K_{\phi\phi}]$ are the elastic and dielectric stiffness matrices respectively; $[K_{u\phi}]$ and $[K_{\phi u}]$ are the piezoelectric stiffness matrices; and the various column matrices on the right-hand side are load vectors. The stiffness matrices are given by

$$\begin{aligned}[K_{uu}] &= \int_V [B_u]^T [c^E] [B_u] dV, & [K_{u\phi}] &= \int_V [B_u]^T [e]^T [B_\phi] dV, \\ [K_{\phi u}] &= \int_V [B_\phi]^T [e] [B_u] dV, & [K_{\phi\phi}] &= - \int_V [B_\phi]^T [\epsilon^S] [B_\phi] dV,\end{aligned}\quad (38)$$

and the load matrices are given by

$$\begin{aligned}\{F\} &= \int_S [N_u]^T \{t\} dS, & \{F_s\} &= \int_V [B_u]^T [c^E] \{S^s\} dV, \\ \{Q\} &= - \int_S \{N_\phi\} q dS, & \{Q_s\} &= - \int_V [B_\phi]^T \{p^s\} dV, \\ \{C\} &= \int_V [B_\phi]^T [e] \{S^s\} dV.\end{aligned}\quad (39)$$

Now the model developed in the previous sections is implemented in a finite element mesh of many crystallites. For the purpose of illustration, all the simulations presented here were carried out for a 2-D ceramic specimen of 93 crystallites. A random number generator is used to generate the crystal axes for all the crystallites. Since it is a 2-D analysis, each crystallite has only four distinct types of variants in the x_1x_2 -plane. A crystallite is modeled as a regular hexagon and each regular hexagon is partitioned into 12 triangle finite elements. Six of the finite elements are located near triple points and the rest of them are around the center of the hexagon, as shown in Fig. 1. A triangle element has a linear interpolation of displacement and potential and hence the strain and electric field intensity is constant within the element. Considering the symmetry of the problem, we have carried out simulations only for a quadrant of the whole ceramic specimen, as shown in Fig. 1. Mechanically, the bottom line $x_2 = 0$ is constrained to zero displacement in the x_2 -direction and the vertical line $x_1 = 0$ is constrained to zero displacement in the x_1 -direction. The other boundary lines $x_1 = L_1$ and $x_2 = L_2$ are free of traction. Electrically, the bottom line $x_2 = 0$ has zero

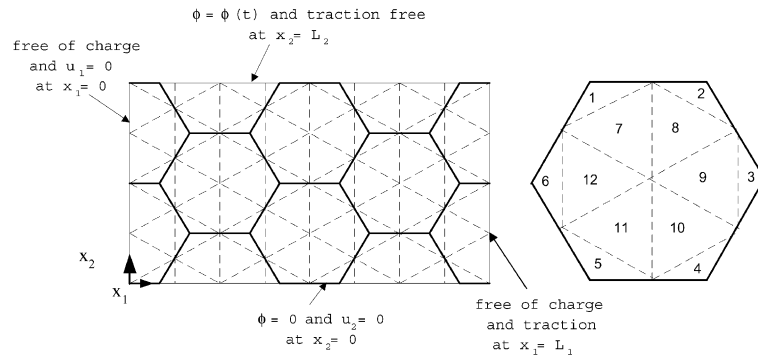


Fig. 1. A schematic diagram of the triangle finite elements.

potential all the time and the top line $x_2 = L_2$ has a given potential $\phi(t)$. The two lines $x_1 = 0$ and $x_1 = L_1$ are free of charge.

We now explain the numerical algorithm that is used to calculate the response of the model under the application of electric field. A similar algorithm is used in calculating the response of the model under mechanical loads. Initially every finite element in the specimen consists of four distinct types of variants, all the variants having the same value of mass fraction. The net polarization of the specimen is therefore zero at the initial instant of time. The electric potential is imposed on the top and bottom lines of the specimen. The potential at the nodes on the line $x_2 = 0$ is kept at zero all the time while the potential $\phi(t)$ at the nodes on the line $x_2 = L_2$ is increased (or decreased) linearly with time. Now we describe the calculation procedure at a time step from t to $t + \Delta t$. Suppose we know the values of all system parameters at time t and the potential at the top line is increased from $\phi(t)$ to $\phi(t + \Delta t)$. What we have to do is to find out the system configuration at time $t + \Delta t$, i.e., the values of mass fraction at time $t + \Delta t$ at every finite element.

(i) First we compute a new set of nodal potentials and displacements, strain and electric field intensity, stress and electric displacement corresponding to the potential boundary conditions at time $t + \Delta t$.

Since the potential boundary conditions at the nodes on the top line have been changed, the finite element equations (37) must be solved to get a new set of nodal potentials and displacements. The strain and electric field intensity can be calculated from Eq. (35) using the new values of nodal potentials and displacements. The electric displacement and stress in an element are given by Eq. (36).

(ii) Compute the Gibbs free energy of distinct types of variants and driving forces in each element and rearrange all the elements in the order of maximum driving force. Calculate the total Gibbs energy of the ceramic body and denote it as $g(0)$.

Substituting the values of electric field and stress into Eq. (10) gives the new values of Gibbs free energy of various types of variants and those values determine the relative stability of variants. In order to apply the switching criterion and kinetics, we have to find out which finite element is more likely to switch. Since the element with a larger maximum driving force is more likely to switch than the element with a lower maximum driving force, it is necessary to rearrange all the finite elements in the order of maximum driving force. Before applying the switching criterion and kinetics, we calculate the total Gibbs free energy of the body by summing up the free energy of all finite elements and call it $g(0)$, where zero in the parenthesis means no switching occurred yet in the elements of the specimen.

(iii) Apply the switching criterion and kinetics to the element with the largest maximum driving force. Then update the mass fractions and material properties of the element and solve the finite element equations again. Using the new set of nodal potentials and displacements, compute the total Gibbs energy $g(1)$, where 1 means that the most-probable element is switched.

The switching criterion (28) and kinetic relation (29) are applied to the element with the largest maximum driving force. The rate of increase of mass fraction of each variant in the finite element is computed from Eq. (30). The values of mass fraction in the element are updated and accordingly the material properties of the element are recomputed using Eq. (17). Then the finite element equations (37) are assembled again using the new values of material properties and solved to yield a new set of electric field and stress fields in the body. As we did in computing $g(0)$, we compute the total Gibbs free energy of the body and call it $g(1)$, where the number 1 in the parenthesis means the kinetic relation is applied to the most-probable finite element.

(iv) Apply the switching criterion and kinetics to the first n most-probable finite elements, where $n = 2, 3, \dots, N_{\text{nucl}}$, and compute the total Gibbs energy $g(n)$, where n is the number of elements to which kinetics are applied.

The second most-probable finite element is switched according to Eqs. (28)–(30), and the values of mass fraction in the element are updated. Then we reassemble the finite element equations and solve them, yielding a new set of electric and stress fields. As before, we compute the new value of total Gibbs energy and call it $g(2)$, where the number 2 means the first and second most-probable elements are switched. In this way we proceed until all the elements satisfying the switching criterion are switched. If N_{nucl} elements satisfy the switching criterion, then we have to repeat the same calculation N_{nucl} times.

(v) Determine the system configuration at time $t + \Delta t$ and go back to (i) for next step calculation.

Our kinetics require that the system configuration at time $t + \Delta t$ should have the lowest total Gibbs energy among $g(0), g(1), \dots, g(N_{\text{nucl}})$. If $g(0)$ is the lowest, then the system does not switch at all at this time step and the values of mass fraction in each element at time $t + \Delta t$ are the same as those at time t . If $g(m)$ is the lowest, then the first m most-probable elements are switched and this becomes the system configuration at time $t + \Delta t$. After finishing the calculation for the time period from t to $t + \Delta t$, the applied potential is increased from $\phi(t + \Delta t)$ to $\phi(t + 2\Delta t)$ and the same calculation procedure is repeated to find the system configuration at time $t + 2\Delta t$.

6. Results and discussion

In previous sections we have developed a general 3-D constitutive and finite element equations for polarization switching of ferroelectric ceramics. Now in this section we apply the developed 3-D formulations to a 2-D example problem. Since it is a 2-D analysis, we need material properties in the x_1x_2 -plane. In the model each crystallite has a randomly generated unique orientation with respect to the global x_1x_2 -axes. Therefore we first give the values of components of material property tensors in the principal crystallographic axes c and a of the tetragonal lattice, which are denoted as the 1 and 2 axes respectively. Then we transform them to the values corresponding to the global x_1x_2 -axes by the tensor transformation rule. We chose a BaTiO₃ ceramic for our calculation and its material properties were taken from Table 5.C. in Jaffe et al. (1971). Those values are as follows:

$$\begin{aligned} \epsilon_1 &= 1.2567 \times 10^{-8} \text{ C/V m}, & S_1^s &= 2.36965 \times 10^{-3}, & p^s &= 0.26 \text{ C/m}^2, \\ \epsilon_2 &= 1.1151 \times 10^{-8} \text{ C/V m}, & S_2^s &= -2.36965 \times 10^{-3}, & \epsilon_0 &= 8.85 \times 10^{-12} \text{ C/V m}, \\ e_{11} &= 18.6 \text{ C/m}^2, & e_{12} &= -4.4 \text{ C/m}^2, & e_{21} &= 11.6 \text{ C/V m}^2, \\ c_{11} &= 162 \times 10^9 \text{ N/m}^2, & c_{12} &= 77.5 \times 10^9 \text{ N/m}^2, & c_{33} &= 42.9 \times 10^9 \text{ N/m}^2, \\ c_{22} &= 166 \times 10^9 \text{ N/m}^2, & & & & \end{aligned} \quad (40)$$

where we have used the contracted notation by converting $11 \rightarrow 1$, $22 \rightarrow 2$, and $12 \rightarrow 3$. In Eq. (40) c_{ij} are the elastic stiffness coefficients at constant electric field; e_{ij} are the piezoelectric coefficients between strain and electric field; and ϵ_i are the permittivities at constant strain. The values of spontaneous strains S_1^s and S_2^s are taken so that the initial net strains of the specimen are zero when the initial value of mass fraction of

each type of variant in an element is 0.25. The amplitude and frequency of applied electric field are $E_{\text{amp}} = 15 \times 10^5$ V/m and 60 Hz, respectively. For simplicity the values of f_{nucl} in Eq. (28) and f_{cr} in Eq. (29) are taken to be equal. With this assumption a variant nucleated at $f = f_{\text{nucl}}$ will grow only when f increases further above f_{nucl} . If f stays at f_{nucl} then the variant does not grow any longer. The value of critical driving force for switching criterion and kinetics may be approximated from the response of a BaTiO₃ single crystal plate. The coercive field of the crystal may be approximated to be 10^5 V/m from Fig. 5.14 in Jaffe's book. Assuming that the effect of stress is negligible in a domain switching of a single crystal plate, the Gibbs energy difference between the two types of variants involved in the domain switching of Fig. 5.14 in Jaffe's book would be approximately given by $E \times p^s$ from Eq. (10). Therefore the values of f_{cr} and f_{nucl} in Eqs. (28) and (29) are approximately

$$f_{\text{cr}} = f_{\text{nucl}} = 26000 \text{ J/m}^3. \quad (41)$$

The proportional constants R_{ij} in Eq. (29) are assumed to have the same value for all kinds of domain switching. Its value is chosen arbitrarily so that it produces reasonable responses. It is $R_{ij} = 5 \times 10^{-4} \text{ m}^2/\text{Ns}$.

Fig. 2 shows the electric displacement versus applied electric field responses of the model at different rates of applied electric field. Since the values of mass fraction of four different types of variants are taken to be 0.25 at the initial instant of time in every finite element, the initial value of net polarization intensity of the body is zero. From the figures we find that the slopes of the curves are relatively large during the initial period of the loading process, but soon the curves get flat during the middle period, and finally near the end of switching the response curves become again steep. It is because in some crystallites there exist two types of variants having almost equal value of free energy under applied field and therefore a much larger field should be applied for a domain switching between the two variants to be finished. This will be discussed further in Fig. 4 in terms of changes in the mass fractions of variants. Fig. 2 also shows the rate dependence of domain switching. As the rate of applied electric field increases, the hysteresis loop is rotated in the counterclockwise direction and the coercive field becomes larger. This rate-dependent behavior has been observed in many experiments, but its simulation in continuum scale has never been done before. This is the first successful simulation of the behavior at the continuum scale.

Fig. 3 shows the applied field-longitudinal strain responses of the model. Due to the shape of the curve, it is often referred to as the butterfly curve. This interesting response is generated mainly by the mass fraction

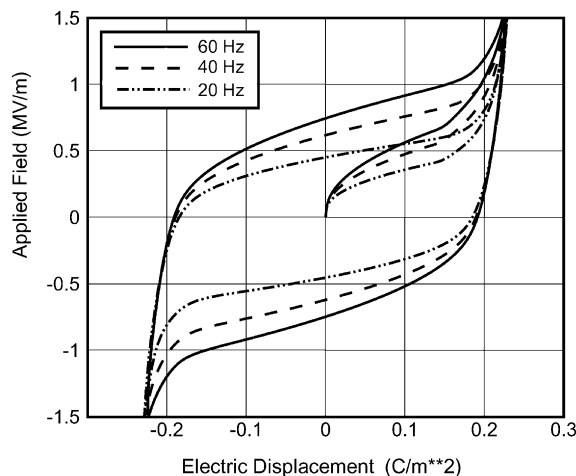


Fig. 2. Electric displacement–applied field responses at three different electrical loading rates.

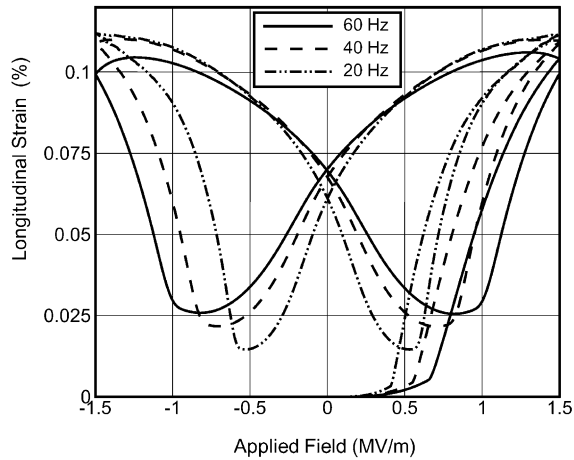


Fig. 3. Applied field–longitudinal strain responses at three different electrical loading rates.

change during a domain switching. As the applied field changes, the values of mass fractions in each element change according to the switching criterion and kinetics. In each finite element there exist four variants with distinct polarization directions. Two of them will have a polarization direction more aligned to the x_2 -axis but the other two will be more aligned to the x_1 -axis. We will call the former variants as x_2 -aligned variants and the latter as the x_1 -aligned variants. The longitudinal strain of the body depends on the total mass fraction of x_2 -aligned variants. If the mass fraction of x_2 -aligned variants increases, then the longitudinal strain of the body increases. If the mass fraction decreases, the longitudinal strain also decreases. Since the mass fractions change in a domain switching process, the longitudinal strain of the body also changes in the process. This relation between the longitudinal strain and the mass fraction of x_2 -aligned variants is shown clearly in Figs. 3 and 4. Since the sum of mass fractions of x_2 -aligned variants depends on the rate of applied field, the butterfly responses also depends on the loading rate.

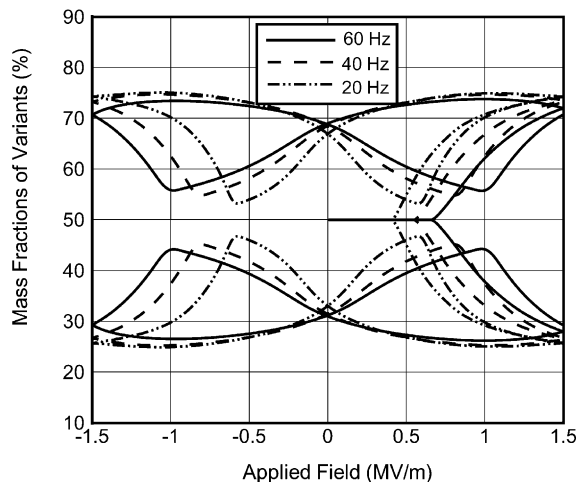


Fig. 4. Change of mass fractions of variants at three different electrical loading rates.

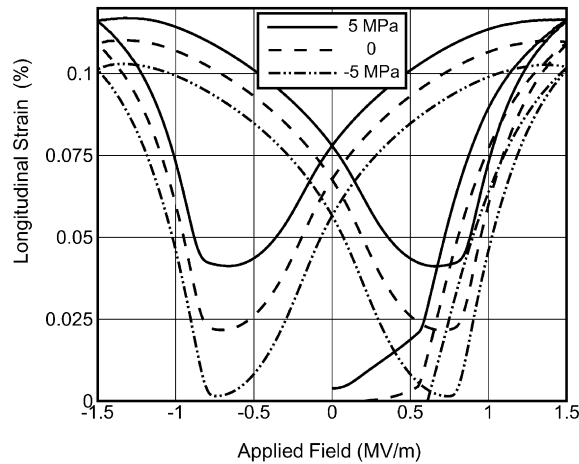


Fig. 5. Effects of stresses applied parallel to the x_2 -axis on the applied field–longitudinal strain responses.

Fig. 4 shows the changes in the total mass fractions of the body during an electrical loading–unloading process. The upper three curves correspond to the mass fractions of x_2 -aligned variants and the lower ones correspond to the mass fractions of x_1 -aligned variants. The sum of the mass fractions of the four variants in a finite element is always 1 and therefore the upper and lower curves are symmetric with respect to the 50% horizontal line in the figure. One may find a great resemblance between Figs. 3 and 4. For example, in the range of applied field between 1 and 1.5 MV/m, the mass fraction of x_2 -aligned variants decreases as the electrical loading rate is increased. This leads to two different phenomena in the same range of electric field: one is the decrease in the longitudinal strain of the body with the increase in loading rate as shown in Fig. 3 and the other is the decrease in longitudinal electric displacement with the increase in loading rate as shown in Fig. 2.

Fig. 5 shows the effects of applied stress on the applied field–longitudinal strain responses when the electrical loading rate is 40 Hz. The external stress is applied on the top surface of the body in the direction parallel to the x_2 -axis. In the figure, the solid line corresponds to the tensile stress of 5 MPa, the dashed line to the zero stress, and the dashed and dotted one to the compressive stress of -5 MPa. It is shown that the longitudinal strain of the body is bigger under the tensile stress than under the compressive one. This can be explained in terms of the change of mass fractions of x_2 -aligned variants shown in Fig. 6. The mass fraction of x_2 -aligned variants, shown in the upper parts of the figure, is bigger when the applied stress is tensile than when the stress is compressive. This naturally leads to a bigger longitudinal strain at a tensile stress. In addition, this results a bigger longitudinal electric displacement at a tensile stress, which we did not show here because they do not differ much on the scale of the figure.

Fig. 7 shows the longitudinal strain–applied stress responses when a ferroelectric domain switching is induced by applied stress parallel to the x_2 -axis under no electric field. The solid line corresponds to the mechanical loading rate of 20 Hz, the dashed one to 2 Hz, and the dashed and dotted one to 0.2 Hz. As it is in the field-induced domain switching of Fig. 2, the size of hysteresis loop gets bigger when the mechanical loading rate is increased. However, the degree of rate-dependency becomes negligible as the loading rate becomes smaller. This rate dependency can also be explained by the mass fraction change during the domain switching process, which is shown in Fig. 8. In Fig. 8, the curves increasing from bottom to top with the increase in applied stress represent the mass fraction of x_2 -aligned variants and the others represent the mass fraction of x_1 -aligned variants. As the applied stress is increased, the x_1 -aligned variants are switched to x_2 -aligned variants and therefore the mass fraction of x_2 -aligned variants increases and this leads to the

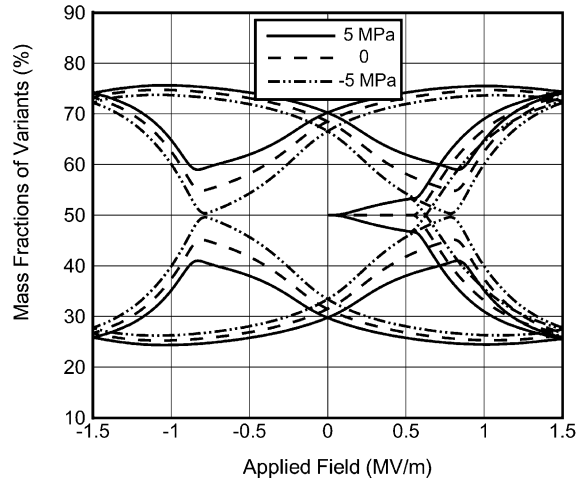


Fig. 6. Change of mass fractions of variants at three different stresses applied parallel to the x_2 -axis.

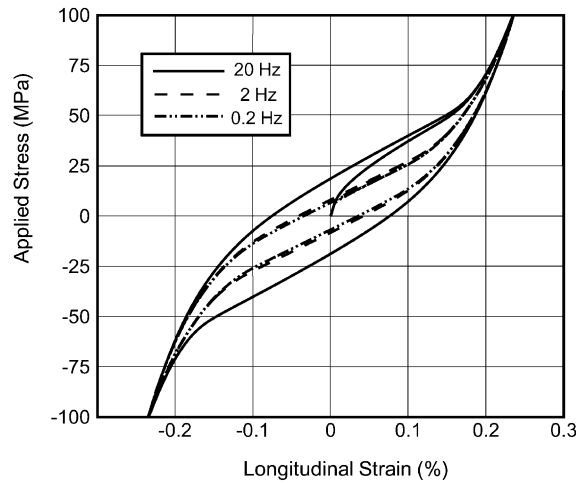


Fig. 7. Longitudinal strain–applied stress responses at three different mechanical loading rates.

increase in the longitudinal strain of the body. The mass fraction of the variant with upward polarization direction is always equal to that of the variant with downward polarization direction; similarly the mass fraction of the variant with rightward polarization direction is equal to that of the variant with leftward polarization direction. Therefore the electric displacement of the body has been kept at zero at any instant of time of the stress-induced switching process. The simulated results presented in Fig. 5 are qualitatively consistent with the experimental observations by Lynch (1996) and Schäufele and Härdtl (1996). However, experimental results on the dependence of macroscopic response of ferroelectrics upon the mechanical loading rate do not appear to be available.

We have also studied the effects of kinetic material constant R_{ij} and critical driving force f_{cr} on the longitudinal electric displacement–applied field responses. Our results indicate that the larger values of R_{ij} lead to the smaller hysteresis loops (i.e., the smaller values of coercive field), but that the larger values of f_{cr} lead to the larger hysteresis loops (i.e., the larger values of coercive field). We note that the model of Hwang

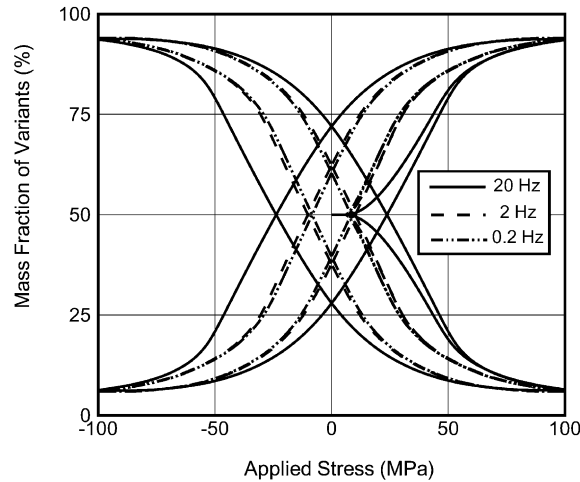


Fig. 8. Change of mass fractions of variants at three different mechanical loading rates.

and McMeeking (1999) also suggests that a larger hysteresis loop corresponds to a larger critical driving force f_{cr} .

7. Concluding remarks

A 3-D continuum model, composed of Helmholtz free energy, switching criterion and kinetics, for polarization switching of ferroelectric ceramics has been presented and implemented into a nonlinear finite element program. The concept of macroscopic particle is used to represent the complicated micro-structures in the material body, and an appropriate nonlinear numerical algorithm is developed based on the total Gibbs energy of the material system. The system configuration at the next time step is the configuration that would give the lowest total Gibbs energy among various possible configurations.

As a demonstration example, the finite element code is applied to a 2-D ferroelectric ceramic. The ceramic body is composed of crystallites with random crystal directions and is subjected to mechanical or electrical loads. The calculation results are in qualitative agreement with experimental observations. Especially, the shape of hysteresis loop is shown to depend mainly on the loading rates. When the electrical loading rate is increased the coercive field is also increased, which is often observed in experiments. Even when the mechanical loads are applied, the response is rate dependent, i.e. the faster loading rate, the bigger hysteresis loop in the stress–strain responses. All these rate-dependent behavior can be explained in terms of the changes in mass fractions of distinct types of variants. Depending on the application direction of mechanical or electrical loads, the most favorable type of variant grows at the expense of other types of variants, leading to the interesting nonlinear behavior of ferroelectric ceramics.

Acknowledgements

Kim would like to acknowledge the support by the University of Seoul (2000), and Jiang acknowledges the support of the US Office of Naval Research through grant N00014-96-1-0884 and the California Space Institute through grant CS-43-98.

References

- Abeyaratne, R., Kim, S.J., Knowles, J.K., 1994. A 1-D continuum model for shape memory alloys. *Int. J. Solids Struct.* 31, 2229–2249.
- Ghandi, K., Hagwood, N.W., 1996. Nonlinear finite element modeling of phase transitions in electro-mechanically coupled material. 96 SPIE Proc. 2715, 121–139.
- Ghandi, K., Hagwood, N.W., 1997. A hybrid finite element for phase transitions in nonlinear electro-mechanically coupled material. 97 SPIE Proc. 2339, 97–112.
- Huo, Y., Jiang, Q., 1997. Modeling of domain switching in polycrystalline ferroelectric ceramics. *J. Smart Mat. Struct.* 6, 441–447.
- Huo, Y., Jiang, Q., 1998. Modeling of domain switching in ferroelectric ceramics: an example. *Int. J. Solids Struct.* 35, 1339–1353.
- Hwang, S.C., Lynch, C.S., McMeeking, R.M., 1995. Ferroelectric/ferroelastic interactions and a polarization switching model. *Acta Metall. Mater.* 43, 2073–2084.
- Hwang, S.C., McMeeking, R.M., 1998. A finite element model of ferroelectric polycrystals. *Ferroelectrics* 211, 177–194.
- Hwang, S.C., McMeeking, R.M., 1999. A finite element model of ferroelastic polycrystals. *Int. J. Solids Struct.* 36, 1541–1556.
- Jaffe, F., Cook, W.R., Jaffe, W.R., 1971. *Piezoelectric Ceramics*. Academic Press, London, New York.
- Jiang, Q., 1993. Macroscopic behavior of a bar undergoing the paraelectric–ferroelectric phase transformation. *J. Mech. Phys. Solids* 41, 1599–1635.
- Jiang, Q., 1994. On the driving traction acting on a surface of discontinuity within a continuum in the presence of electromagnetic fields. *J. Elasticity* 34, 1–21.
- Jiang, Q.Y., Cao, W., Cross, L.E., 1994. Electric fatigue in lead zirconate titanate ceramics. *J. Am. Ceramic Soc.* 77, 211–215.
- Jona, F., Shirane, G., 1962. *Ferroelectric Crystals*. Pergamon Press, New York.
- Kim, S.J., 1998. A simple continuum model for polarization reversals in ferroelectrics. *J. Smart. Mater. Struct.* 7, 572–579.
- Kim, S.J., 2000. A 1-D continuum model for thermoelectric phase transformations in ferroelectrics. *Int. J. Solids Struct.* 37, 1145–1164.
- Lynch, C.S., 1996. The effect of uniaxial stress on the electromechanical response of 8/65/35 PLZT. *Acta Mater.* 44, 4137–4148.
- Schäufele, A., Härdtl, K.H., 1996. Ferroelastic properties of lead zirconate titanate ceramics. *J. Am. Ceramic Soc.* 79, 2637–2640.
- Strukov, B.A., Levanyuk, A.P., 1998. *Ferroelectric Phenomena in Crystals*. Springer, Berlin, Heidelberg.